Search for right-handed currents in the decay $K^+ \to \mu^+ \nu$

T. Yamanaka,* R. S. Hayano, T. Taniguchi,† T. Ishikawa, S. Ohtake,‡ M. Iwasaki, Y. Akiba, and T. Yamazaki

Department of Physics and Meson Science Laboratory, Faculty of Science, University of Tokyo, 7-3-1 Hongo, Bunkyo-ku, Tokyo 113, Japan

S. R. Schnetzer§

National Laboratory for High Energy Physics, Oho-machi, Tsukuba-gun, Ibaraki 305, Japan

(Received 10 January 1986)

The longitudinal polarization of the muon emitted in the decay $K^+ \to \mu^+ \nu$ was measured to search for right-handed weak currents in a strangeness-changing process. The 236-MeV/c muons from the decay of stopped K^+ were identified and were collected by a magnetic spectrometer. The muons were then slowed down in a carbon degrader and were brought to rest in an aluminum target. The muon spins were precessed by a 220-G transverse field, and a muon-spin-rotation technique was employed to measure the muon-spin polarization. The polarization was determined to be -0.970 ± 0.047, which is consistent with the $V-A$ hypothesis.

I. INTRODUCTION

Our current understanding of the electroweak interactions is based on the successful "standard model."[1-3] At present, there seems to be no compelling evidence against the $SU(2)_L \otimes U(1)$ description of the interactions. However, on a closer look, we realize that some of the limits imposed by experiments are not stringent. For example, how are we sure that the weak interaction is *purely* left handed? Is it really true that there is no such thing as a right-handed neutrino?

The left-handedness of the weak interactions has long been established,[4-7] and is built into the "standard model" *by hand;* the model does not explain why the right-handed sector is missing. Left-right-symmetric models based on the $SU(2)_L \otimes SU(2)_R \otimes U(1)$ gauge group[8] are appealing since they "explain" why we only see left-handed weak interactions. In these models, the left-handedness is provided if the spontaneous symmetry breaking gives a larger mass to the right-handed gauge boson (W_R) than to the left-handed gauge boson (W_L), thereby suppressing the effects due to the right-handed currents. In this scheme, the right-handed current is not *missing* but is just *suppressed* [by an order $(m_{W_L}/m_{W_R})^2$]. How can we detect the effects of right-handed currents?

As is well known, the muons in the decays $\pi^+ \to \mu^+ \nu$ and $K^+ \to \mu^+ \nu$ are purely left-handed if the interaction is $V-A$, and if the neutrino is massless (Fig. 1). If the decays are mediated by W_R and if right-handed neutrinos are emitted, the muon spins are oppositely polarized. Therefore, the admixture of right-handed currents results in the reduction of the muon longitudinal polarization P_μ.

The muon polarization P_μ can be measured by using the angular asymmetry of the positrons in the decay $\mu^+ \to e^+ \nu \bar{\nu}$. This angular asymmetry is represented by a muon-decay parameter ξ, which is $+1$ (-1) for the left- (right-) handed process; thus a precise determination of ξ can tell us whether or not the weak currents involve right-handed component. Note that P_μ and ξ cannot be measured separately.

For pion decay, recent measurements[9,10] at TRIUMF have greatly improved the limit of $\xi P_\mu \delta/\rho$ to < -0.9966 (90% C.L.) over the previously known value[11] $\xi P_\mu = -0.972 \pm 0.013$, where δ (0.7551 ± 0.085) and ρ (0.7517 ± 0.0026) are muon-decay parameters.[12] For kaon decay, the ξP_μ values are -0.96 ± 0.12 (Ref. 13), -0.94 ± 0.21 (Ref. 14), and -1.0 ± 0.1 (Ref. 15). It should be noted that the left-handedness in kaon decay was only determined with an accuracy of 10%.

The muon polarization in pion decay and kaon decay carries different information. As shown in Fig. 2, the coupling factor is proportional to $(g/m)^2 \cos\theta$ for pion decay, and $(g/m)^2 \sin\theta$ for kaon decay, where g is the weak coupling constant, m is the mass of the weak gauge boson, and θ is the Cabibbo angle. In the left-right-

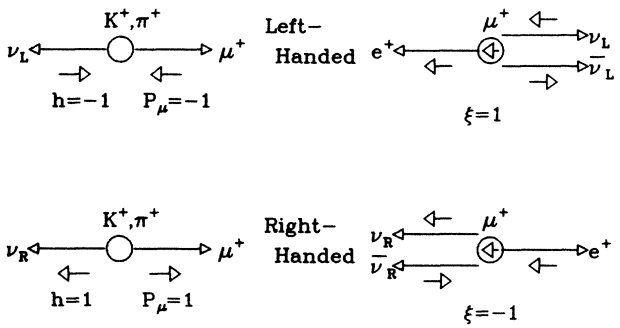

FIG. 1. In the decays $\pi^+ \to \mu^+ \nu$ and $K^+ \to \mu^+ \nu$, the muon and the neutrino have the same helicity. If there is a contamination of the right-handed weak current in the decay, then the right-handed neutrino will be produced, and it can be detected as a reduction of the muon polarization. The asymmetry of the decay $\mu^+ \to e^+ \nu \bar{\nu}$ also shows the neutrino helicity directly.

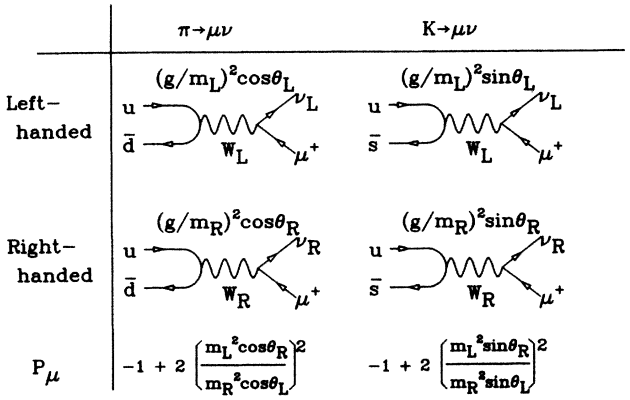

FIG. 2. Feynman diagrams of the decays $\pi^+\to\mu^+\nu$ and $K^+\to\mu^+\nu$ are shown for left- and right-handed currents. The coupling constant of the decay is proportional to the factor written for each diagram. Here, m is the mass of the weak gauge boson, θ is the Cabibbo angle, and g is the weak coupling constant. The suffixes L and R denote the left- and right-handed sectors, respectively.

symmetric model, m and θ can be different between left- and right-handed sectors. The ratio of right-handed currents to left-handed currents would be proportional to $(m_L/m_R)^2(\cos\theta_R/\cos\theta_L)$ for pion decay, and $(m_L/m_R)^2(\sin\theta_R/\sin\theta_L)$ for kaon decay. Therefore, two independent measurements for $\Delta S=0$ (π decay) and $\Delta S=1$ (K decay) are needed to extract limits on the mass of the right-handed gauge boson, and to determine the right-handed quark-mixing angle. In the extreme case of $\theta_R=90°$, the effects of right-handed currents can only be observed in kaon decays. This is the motivation to search for right-handed currents in the kaon decay. A brief account of the result of this experiment was already published.[16]

II. PRINCIPLE OF THE EXPERIMENT

In order to search for right-handed currents in the kaon decay, we measured the longitudinal polarization of the muon emitted from the decay $K^+\to\mu^+\nu$ ($K_{\mu 2}$) as follows: (i) stop K^+, (ii) identify and collect the $K_{\mu 2}$ muons by using the unique momentum 236 MeV/c, (iii) slow down the muons and stop them in a spin-precession target, and (iv) measure the muon polarization from the angular asymmetry of the positrons emitted in the decay $\mu^+\to e^+\nu\bar{\nu}$, by using the muon-spin-rotation (μSR) technique.

A. Identification and collection of muons

Positive kaons were stopped in a target counter assembly, and the $K_{\mu 2}$ decay muons were identified and were collected by using a magnetic spectrometer. The momentum was analyzed by measuring the track. After passing through the magnet, the muons were focused to an apparatus for measuring the polarization.

B. Initial muon spin direction

The initial muon spin direction was determined by measuring the muon momentum direction at the exit of the spectrometer. Here, we assumed that the muon spin kept up with the momentum bending, since the cyclotron frequency and the spin-precession frequency are practically the same. The depolarization of the muons during the subsequent slowing down process was minimized by using carbon as the degrader material (see Appendix A for details).

C. Muon-stopping target

We used a pure (99.99%) aluminum plate as the muon-stopping target. Since the loss of muon polarization in the target can simulate the existence of right-handed currents, the selection of the target material was crucial. The selection criteria are as follows. (a) There is no fast initial depolarization, as caused by the formation of muoniumlike states, (b) there is no paramagnetic or spin-lattice depolarization, (c) the material is low Z so that energy loss and multiple scattering of the decay positrons can be minimized, and (d) the material is stable and needs no container.

As shown in Table I, aluminum is known to exhibit a long relaxation time, and it meets all the above conditions. Although aluminum nuclei have nonzero magnetic moments, muons are believed to be diffusing fast enough so that they are free from relaxation.

D. Muon decay

The muon polarization was measured by using the angular asymmetry of the decay $\mu^+\to e^+\nu\bar{\nu}$. The positron

TABLE I. The damping parameter of muon-spin relaxation in various materials near room temperature. The damping parameter Λ is defined as the reciprocal of the time period when the asymmetry becomes $1/e$.

Material	Λ (μsec^{-1})	Temperature (K)	Reference
Al	0.009±0.005	300	17
	0.003±0.007	290	18
	0.024±0.007	90	19
	0.039±0.010	0.5	20
Cu	0.038±0.009	300	17
	0.012±0.006	293	21
	0.18 ±0.005	135	22
	0.25 ±0.13	90	19
V	0.088±0.008	300	17
	−0.002±0.008	290	23
	0.1 ±0.02	200	21
	0.25 ±0.006	80	22
Nb	0.023±0.005	280	24
	0.22 ±0.006	85	22
	0.39 ±0.16	55	23
Ta	−0.005±0.008	300	17
	0.006±0.006	110	21

emission favors the direction of the muon spin, especially at higher energies. The differential decay probability for a positron emitted at an angle θ with respect to the muon spin direction is given by

$$dW(x,\theta) \propto [I(x) - \xi P_\mu C(x)\cos\theta]dx\, d\theta\ , \tag{1}$$

where

$$\begin{aligned} &x = E_e / E_e^{\max}\ , \\ &E_e = \text{positron energy},\quad E_e^{\max} = 53\ \text{MeV}\ , \\ &I(x) = 2[3(1-x) + 2\rho(4x/3 - 1)]x^2 \\ &\qquad\qquad\qquad\qquad \text{(isotropic term)}\ , \\ &C(x) = 2[(1-x) + 2\delta(4x/3 - 1)]x^2 \\ &\qquad\qquad\qquad\qquad \text{(cosine term)}\ . \end{aligned} \tag{2}$$

Here, ξ represents the asymmetry of muon decay, and P_μ is the muon polarization. If the interaction is pure $V-A$, the muon decay parameters are $\xi = 1$ and $\rho = \delta = \frac{3}{4}$.

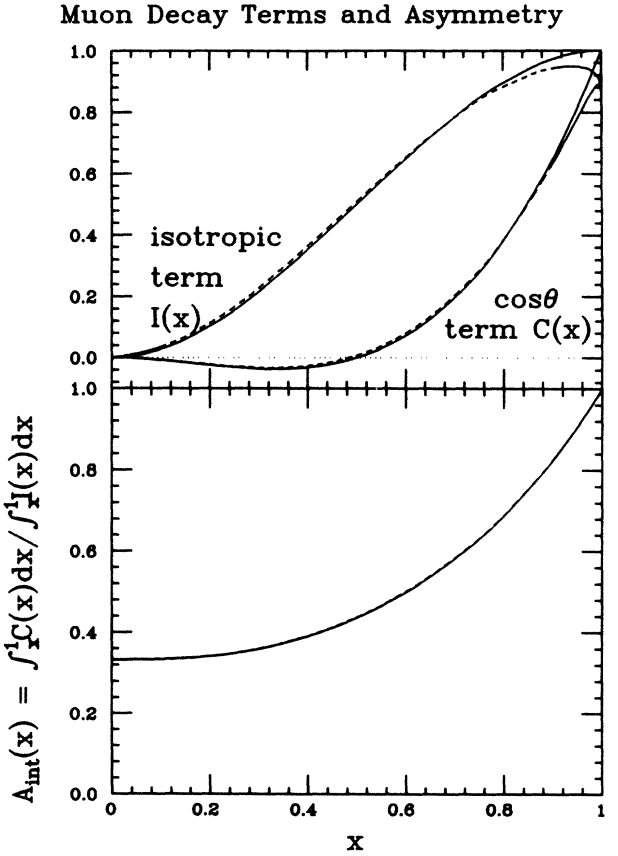

FIG. 3. The top shows the isotropic and cosine terms of muon decay in Eq. (2), where x is the normalized energy of the positron (maximum energy = 1.0). The solid (dashed) line shows the terms with (without) radiative corrections. The bottom shows the asymmetry of positrons above energy threshold x. Note that radiative corrections do not contribute significantly to the asymmetry.

E. Measurement of μ-decay asymmetry

In order to measure the muon-decay asymmetry, we integrated the positron spectrum over the energy, instead of measuring the energy of each positron. The energy threshold was set as low as 1 MeV, to reduce the systematic errors caused by fluctuation and error of the threshold.

Let us introduce an energy-integrated asymmetry $A_{\text{int}}(x)$, which is the asymmetry of positrons above the energy threshold x, as

$$A_{\text{int}}(x) = \frac{\int_x^1 C(x)dx}{\int_x^1 I(x)dx}\ . \tag{3}$$

The $A_{\text{int}}(x)$ is shown in Fig. 3 as a function of x. The asymmetry is $\frac{1}{3}$ for all positrons ($x=0$), and grows to 1 for those with the maximum energy ($x=1$). Although the asymmetry is larger at higher energies, the steepness of the curve is likely to introduce a systematic error. In Fig. 4, the energy resolution Δx is shown as a function of x for several values of the polarization accuracy ΔP. If we measure the asymmetry with 1% of accuracy at the end-point energy ($x=1$), then we should know the energy threshold within an accuracy of $53 \times 0.5\% = 0.3$ MeV. On the other hand, if we set the energy threshold at 2 MeV ($x=0.04$), then we can achieve the same accuracy even with an accuracy of $53 \times 13\% = 6.9$ MeV.

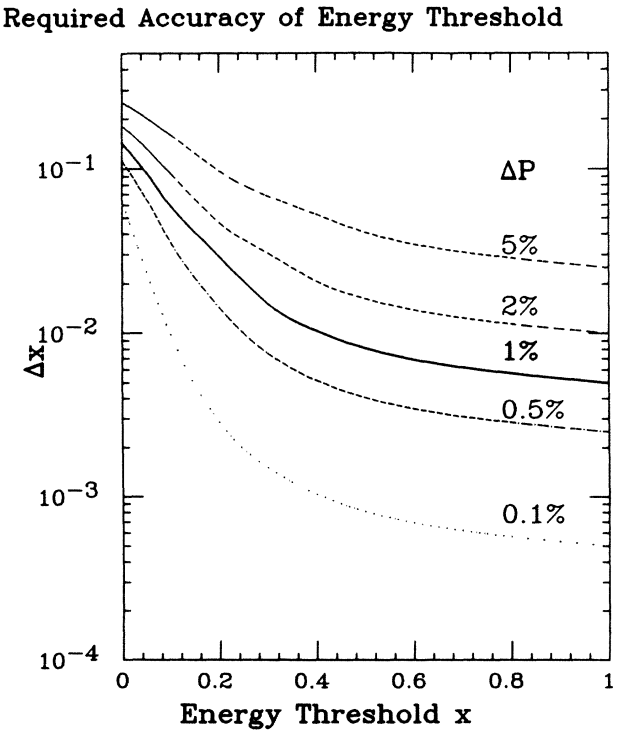

FIG. 4. Required accuracy of energy threshold is shown as a function of the threshold, for some polarization errors. If we were to measure the asymmetry to 1% at the end-point energy ($x=1$), then the energy threshold should be known within 0.3 MeV. The same accuracy can be obtained by setting the energy threshold as low as possible, even if the error in the energy determination has an uncertainty of 6.9 MeV.

F. μSR

The muon-spin-rotation (μSR) method was used to measure the polarization. In this method, a transverse magnetic field is applied to the muon to precess the spin. The muon polarization is determined by the amplitude of the oscillatory pattern of the decay positron time spectrum. This method is relatively free from systematic errors, since the same counter (thus the same solid angle, same energy threshold, etc.) is used to measure the positron spectrum.

Integrating the muon decay rate (1) over the positron energy, the rate is

$$dW(\theta) \propto (1-\xi P_\mu/3\cos\theta)\sin\theta\, d\theta\ . \tag{4}$$

If we apply a magnetic field B, when the muon spin precesses around the field vector. The precession frequency is

$$\begin{aligned}\omega(B) &= g\,eB/(2mc)\\ &= 2\pi\times 13.553\times 10^3 B\ \text{rad/G sec}\\ &= \Omega B\ ,\end{aligned} \tag{5}$$

where g is the g factor and m is the mass of the muon.

If we place a positron counter at an angle ϕ, with respect to the initial muon spin, then the observed angle between the muon spin and the positron direction θ, at time t, will be

$$\theta = \omega t - \phi\ . \tag{6}$$

Therefore, the number of observed positrons $dN(t,\phi)$ oscillates with the precession frequency, and decreases exponentially as

$$dN(t,\phi) = n_0[1-\xi P/3\cos(\omega t-\phi)]\exp(-t/\tau)dt\ , \tag{7}$$

where τ ($=2.2$ μsec) is the lifetime of the muon.

III. EXPERIMENTAL APPARATUS

The experiment was performed at the K3 beam channel[25] of the 12-GeV proton synchrotron at the National Laboratory for High Energy Physics (KEK). The key points of the experiment are (i) kaon beam, (ii) stopping kaons, (iii) selecting $K_{\mu 2}$ muons, (iv) stopping muons, (v) measuring muon polarization, (vi) trigger logic, and (vii) data acquisition. They are described in detail in the following sections.

A. Kaon beam

Figure 5 shows a plan view of the K3 beam channel. A platinum target was placed in the proton beam line extracted from the 12-GeV proton synchrotron. Kaons around a momentum of 550 MeV/c were transported to the experimental area through the K3 beam line. The momentum of the particles was selected by a bending magnet $D1$ and a momentum slit at a momentum-dispersive intermediate focusing point. The mass of the particles were selected by a dc separator, and a mass slit at the intermediate focus. The dc separator supplied a high voltage of 600 kV in the vertical direction (by two electrodes 15 cm apart, and 1.88 m long) and a cross magnetic field of 180 G, which allowed 550-MeV/c kaons to go straight through. The selected kaons were then focused on a kaon-stopping target by a bending magnet $D2$ and four quadrupole magnets $Q5$–$Q8$.

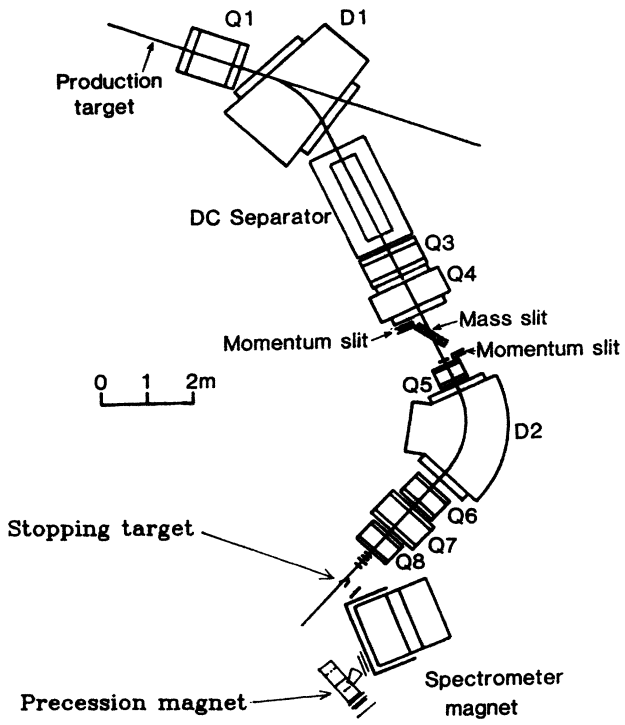

FIG. 5. Plan view of the K3 beam line of the proton synchrotron at the National Laboratory for High Energy Physics. The kaons with a momentum of 550 MeV/c were selected by an electrostatic separator, mass and momentum slits, and were focused on a kaon-stopping target.

Figure 6 shows a plan view of the experimental apparatus. A total reflection-type Lucite Čerenkov counter (AC) with 5 cm thickness was placed after $Q8$ to veto

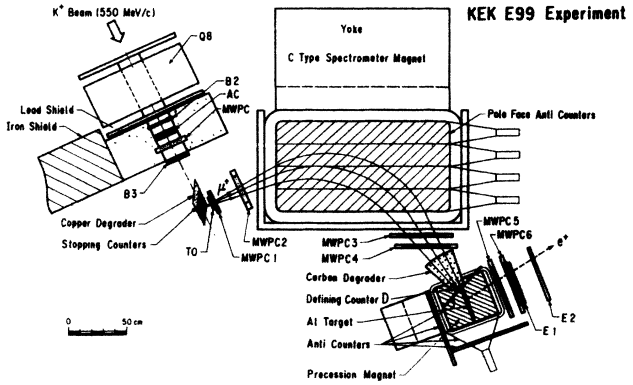

FIG. 6. Plan view of the experimental setup. The kaons were identified by a Lucite Čerenkov counter AC slowed down by a copper degrader, and stopped in the stopping counters. The decay muons were focused on an aluminum target by using the spectrometer magnet.

pion contamination in the beam. The Čerenkov counter had a total reflection threshold of $\beta = 0.91$ for normal incidence, while the pions and kaons had β's 0.98 and 0.74, respectively. The efficiency of the counter for pions was 99.8%. A counter $B3$ was placed after the Čerenkov counter to determine the incident timing of the kaons.

The numbers of kaons and pions were measured by counting the rates $B2 \cdot \overline{AC} \cdot B3 \cdot \mathrm{ST1}$ and $B2 \cdot AC \cdot B3 \cdot \mathrm{ST1}$, respectively, where ST1 is the first kaon-stopping counter. There were 2×10^4 kaons and 8×10^4 pions per 1×10^{12} protons.

B. Stopping kaons

A degrader and a kaon-stopping target were placed at the final focusing point of the K3 beam line.

The kaon degrader consisted of a copper plate of 3 cm thickness, tilted by 30 degrees with respect to the beam line, thus the effective thickness was 6 cm (54 g/cm^2).

The kaon-stopping target consisted of seven layers of 6-mm-thick plastic scintillators, which were also tilted by 30° with respect to the incoming beam. All the layers of the stopping counters (ST1—ST7) were required to give signals when a kaon stopped in any of the layers and a muon emerged toward the spectrometer. The energy deposits of kaons and muons in each counter were about 20 and 0.3 MeV, respectively. In order to cover this wide energy range, anode and dynode signals from each stopping counter were fed into analog-to-digital converters (ADC's). The anode signal had a narrow energy range (0—4 MeV) for the muons, while the dynode signal covered a wide energy range (0—60 MeV) for the kaons.

C. Selection of muons

As described in the previous section, the spectrometer magnet was used to collect the decay muons and to analyze their momenta. The size of the magnet pole was 80×150 cm^2. The gap between the poles was 21 cm, and a vertical magnetic field of 8 kG was applied. In order to gain a large solid angle by vertical focusing effect at the entrance edge, the averaged injection angle was set at 25 degrees.

The gap between the magnet poles was filled with helium to reduce multiple scattering. Also, the surface of the pole was covered with thin (3-mm-thick) plastic scintillation counters, to veto particles which were scattered by the pole face.

Four multiwire proportional chambers (MWPC1—MWPC4) of bidimensional readout were placed at the entrance and the exit sides of the magnet to determine the muon trajectory. These were used to obtain the muon momentum. The initial axis of the muon spin was assumed to be antiparallel to the muon momentum direction at the exit of the magnet, and was determined by using MWPC3 and MWPC4. The details of the chambers and the method to obtain the hit positions are described in Appendix B.

A counter called $T0$ was placed in front of MWPC1 to trigger on the muons emitted toward the spectrometer magnet.

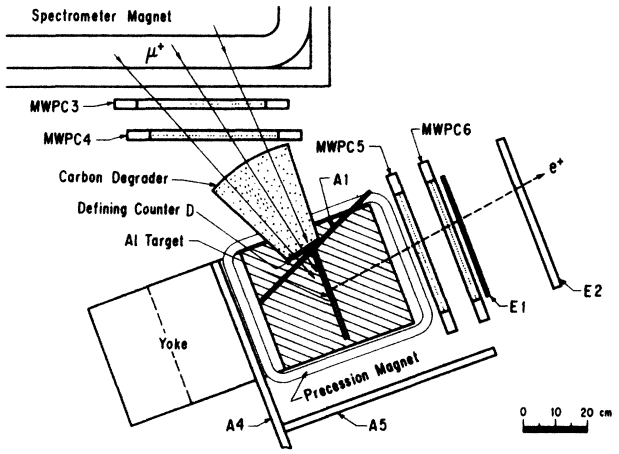

FIG. 7. Close view of the apparatus for measuring the muon polarization. The muons were degraded by a carbon block, and then stopped in the aluminum target. The muon spin was rotated by a magnetic field applied by a precession magnet. The decay positron was detected by a pair of chambers MWPC5, MWPC6 and scintillation counters $E1, E2$.

D. Stopping muons

Figure 7 shows a close-up view of the apparatus downstream of the spectrometer. The muon-stopping target was placed at the focusing point of the muons, and the degrader was placed between the target and MWPC4.

A block of carbon was used for the muon degrader. The degrader was 33.5 cm thick and shaped like a fan, to make the path length almost independent of the trajectory.

A defining counter D (8 cm wide) was placed behind the degrader to select muons which hit the muon-stopping target. The timing of the incoming muon was determined by this counter.

The muon-stopping target consisted of a high-purity aluminum (99.99%) plate. The target had a dimension of 300 (width) $\times$ 350 (height) $\times$ 5 (thickness) mm^3, and was tilted by 70° with respect to the edge of the spectrometer magnet. This tilting angle was determined to maximize the muon-stopping rate. Although a larger thickness would increase the stopping rate, it would obscure the emission angle of the decay positron due to multiple scattering. Therefore, an optimum thickness chosen was a compromise between the above two conditions.

E. Measurement of the muon polarization

The muon-stopping target was placed in a Mylar box filled with helium gas, and the box was placed between the poles of a spin-precession magnet.

The precession magnet with rectangular poles (40×43 cm^2) and with a gap of 40 cm was used to apply a vertical magnetic field to the muon-stopping target. The magnetic field between the poles was mapped by a 5-cm mesh with an accuracy of 1 G. The field at the center region of the target was about 220 G. The field map was used in the analyses to take care of the field inhomogeneity over

the target volume. The shunt voltage of the magnet power supply was monitored for each event. In the later analysis, this was used to correct for the drift of the magnetic field, which was within $\pm 0.1\%$.

The positron arm was placed at one side of the precession magnet edge. A set of chambers (MWPC5, MWPC 6) was used to track the emitted positron in the muon decay. The emission angle of positrons, and the decay position of the muons were obtained from the track measurement. The resolution of the chambers was about 1 mm in σ. The angular resolution was thus about 0.5° for MWPC5 and MWPC6, or only 4×10^{-5} in cosine. On the other hand, the resolution would cause an error in the precession field, by misestimating the decay position. The field gradient for the final available data was about 1.5 G/cm in σ. Therefore, even after 10π of precession, the error would be about 0.1% in cosine.

A pair of scintillation counters ($E1$ and $E2$) were placed behind the chambers, to trigger on positrons. The thickness of the $E1$ counter was 2 mm to reduce the number of positrons stopped in the counter. The decay time of the muon, which is the time difference between the D and $E1$ counters, was measured by counting the output of a 1-GHz pulser [GHz-TDC (time-to-digital converter)]. The solid angle of the positron arm was about 6%. The energy threshold of the positron arm was less than 0.1 MeV.

The muon-stopping target was surrounded by five anticounters ($A1$–$A5$). The purpose of these counters was (a) to reject muons which did not stop in the muon-stopping target, (b) to veto "second" muons which entered into the helium box within 10 μsec, and (c) to veto particles which passed through or scattered at the muon-stopping target and went into the positron arm.

Viewed from the center of the muon-stopping target, these anticounters and the positron arm covered 85% of the solid angle. The energy thresholds of the counters were about 0.1–0.5 times the energy deposit of a minimum ionizing particle.

The Mylar box was filled with helium gas to reduce the multiple-scattering effect of the emitted positrons. The mean angle of the multiple scattering by the gas and the Mylar (6 μm) was 3° even for positrons with the momentum of 2 MeV/c. This introduces an uncertainty of 10^{-3} in cosine, which is negligible in comparison with the statistical error in this experiment.

F. Fast-trigger logic

The schematic diagram of the fast-trigger logic of our experiment is shown in Fig. 8. The outputs of the scintillation counters and the MWPC5 and MWPC6 were discriminated to produce the following logic.

(1) "K": Incident particle was kaon. This was generated by a coincidence of $B2\cdot B3\cdot\overline{AC}$, whose timing was defined by $B3$. The counting rate was 1.6×10^{4} per 1×10^{12} protons.

(2) "Stop": A particle has passed through all the stopping counters and $T0$ counter. This was made by the coincidence of all the stopping counters and $T0$. The discriminated output of the stopping center was set wide

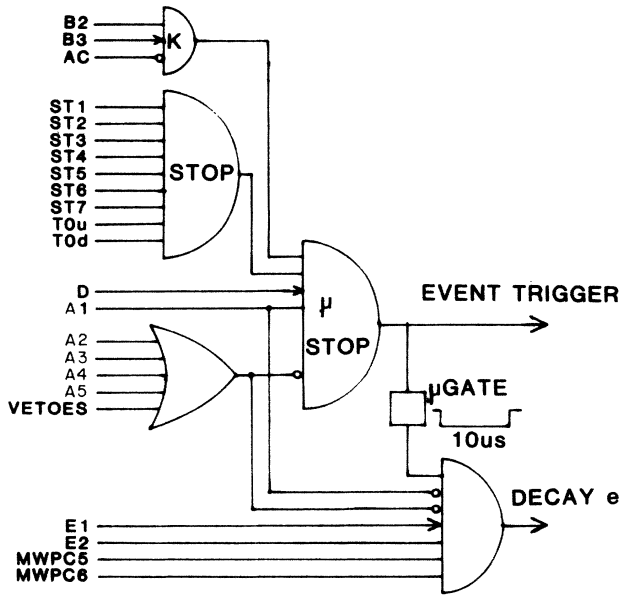

FIG. 8. Diagram of the fast trigger logic. The arrows indicate the signals which determined the timing of the logic. The event trigger was generated when a kaon stopped in the stopping counter, and the decay muon stopped in the aluminum target. The trigger opened a 10-μsec gate to record decay positron.

enough (50 nsec, in comparison with the 12-nsec kaon lifetime), to accept 98% of the decay particles.

(3) "μstop": The decay muon stopped in the muon-stopping target. The logic was generated by "K"·"stop"·$D\cdot A1\cdot\overline{\sum A_i}$ ($i=2,\ldots,5$) with D timing, where D is the signal of the target-defining counter at the downstream of the carbon degrader. This was our "event trigger." The computer trigger, all the TDC start pulses, and ADC gates except for the positron arm counters were gated by this signal. Also a "μgate" with a pulse width of 10 μsec was made to select the decay positron. The rate was 2.2 per 1×10^{12} protons.

(4) "Decay e": A positron from the muon decay entered the positron arm. This signal was made by "μgate"·$E1\cdot E2\cdot PC5\cdot PC6\cdot\overline{\sum A_i}$ ($i=1,\ldots,5$). The chamber signals of $PC5$ and $PC6$ were obtained by discriminating anode output amplified by a factor of 10^3. The GHz-TDC stop signal and ADC gates for the $E1$, $E2$, $PC5$, and $PC6$ were generated by this logic. The rate was 6.5×10^{-2} per 1×10^{12} protons.

Special care was taken to reject muons which did not come through the D counter. If a signal "K"·$A1\cdot\overline{\mu\text{stop}}$ came within ± 5 μsec of a "μstop" signal, then all the ADC's and TDC's were cleared immediately. About 5% of the "μstop" events were rejected by this scheme.

G. Data acquisition

Signals from all of the counters except for the anticounters were put into ADC's and TDC's. The output signals of the chambers were also put into ADC's for cathode readout.

The data-taking system consisted of a PDP-11/34 mini-

computer and a CCS-11 intelligent CAMAC branch diver. They were operated under the KEKX data-taking system.[26] The acquired events were written on to magnetic tapes, while some of them were monitored and analyzed in real time.

The experiment was performed over a two-month period. The effective beam time for the data acquisition was about 30 days. The number of total accumulated events with an $E1$ signal (the event trigger did not require $E1$) was 5.5×10^4.

IV. DATA REDUCTION

Before the final analysis, three cuts were applied to the raw data to select $K \to \mu \to e$ events: (1) select stopped kaons, (2) select muons emitted from $K_{\mu 2}$ decay, and (3) select positrons emitted from the muon decay. The number of events after each cut is summarized in Table II. The number of events surviving these cuts was 9.1×10^3.

A. Selection of the stopped kaons

The stopped kaons were identified by the following criteria: (a) the incoming particle was a kaon, (b) the layer in which the kaon had stopped was well defined, and (c) the muon was emitted after a delayed timing. The kaons had already been selected by the trigger logic, but an additional software cut was applied to reject the surviving pions.

Event by event, particles were identified for each layer by the anode and dynode pulse heights. The stopping layer was determined by finding a layer where all the upstream counters had a kaon and the downstream counters had a decay particle.

The stopping layer was also determined by using the timing. In the stopping counters, the kaons have the same timing as $B3$, and the decay muons have the same timing as the $T0$ counter. The kaon stopping layer was determined by the following two criteria: (i) the most downstream layer which had the same timing as $B3$ and (ii) the one before the most upstream layer which had the same timing as $T0$.

Figure 9 shows the distribution of decay time of the kaons, which was measured by the time difference between the $B3$ and $T0$ signals. In this spectrum, prompt events within 3 nsec were rejected, because they included decay-inflight events, and particles which were scattered in the stopping target and went through the $T0$ counter. The lifetime of the kaons was 12.4 ± 0.2 nsec, which was consistent with the world average (12.37 nsec).

TABLE II. The number of events after each event selection.

Selection	Number of events remaining
Total events	54 813
Chamber reconstruction	33 005
Stopped kaon	29 150
$T0$ and D timing	19 878
Muon momentum	18 630
Positron	14 930
Precession angle	9 134

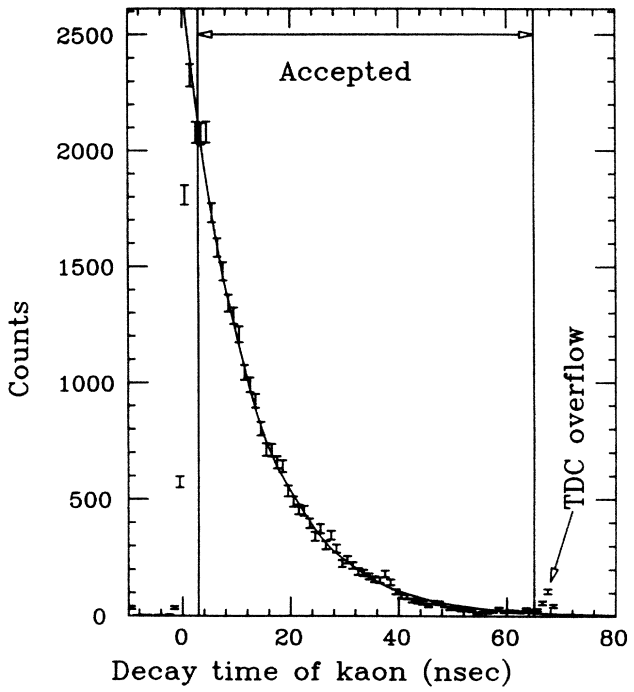

FIG. 9. Time difference between the $T0$ and $B3$ counters. The solid line shows the exponential curve with the fitted lifetime.

B. Selection of the muons

The muons emitted from the decay $K^+ \to \mu^+ \nu$ were selected by their momentum using the following steps: (1) reconstruct the hit positions on the chambers MWPC1–MWPC4, (2) reject particles which hit the magnet or did not come out from the stopping target, (3) reconstruct the momentum, and (4) apply a cut on the momentum.

The hit positions on the chambers were determined from the induced charge on the cathode strips. We used an algorithm developed by Chiba *et al.*[27] All the chambers were required to have a single hit in the horizontal and vertical planes.

The track was extrapolated from MWPC1 and MWPC2 to the surface plane of the last stopping target (ST7). In order to reject background events, the points were required to be within the boundary of ST7. The track was also extrapolated toward the spectrometer magnet. The events which hit or came out from the end guard of the magnet were rejected.

After the track was defined, the momentum p^* of a particle in the spectrometer was calculated by the effective edge method, namely, approximating the field with a step function and calculating the momentum geometrically.

Figure 10 shows the momentum distribution for each kaon-stopping layer. The momentum is lower when the particle was emitted in upstream counters, because the particle lost its energy in the stopping target and the $T0$ counter. The averaged momentum of the muons within ± 10 MeV/c of the peak is indicated by an arrow for each stopping layer. By a linear regression, we see that the

muon lost its momentum by 1.71 MeV/c per layer. Since the observed p^* was effectively the momentum of a particle emitted at the layer 8.5 (the surface of the $T0$), we estimated the initial momentum p by

$$p = p^* + 1.71(8.5 - L) , \tag{8}$$

where L is the stopping layer number. The momentum distribution after this energy-loss correction is shown at the top of Fig. 10. The peak is at 235.3 MeV/c, and the resolution was 1.1% in σ.

The muons emitted from the decay $K^+ \to \mu^+ \nu$ were identified by selecting the momentum within 235.5±5 MeV/c. The contamination of the radiative decay $K^+ \to \mu^+ \nu\gamma$ events was about 0.5%. The contamination of muons from the decay $K^+ \to \mu^+ \nu\pi^0$ was less than 0.05%.

C. Selection of positrons

The positrons emitted from the muon decay were selected by the decay time of the muon, and the decay position. The decay time of the muon was measured by the time difference between the D and $E1$ counters. The timing spectrum is shown in Fig. 11. In order to select stopped muons, the decay time was required to be within 0.055 and 10 μsec. The positron track was extrapolated toward the muon-stopping target. In order to reject background events, the decay point was required to be inside of the target.

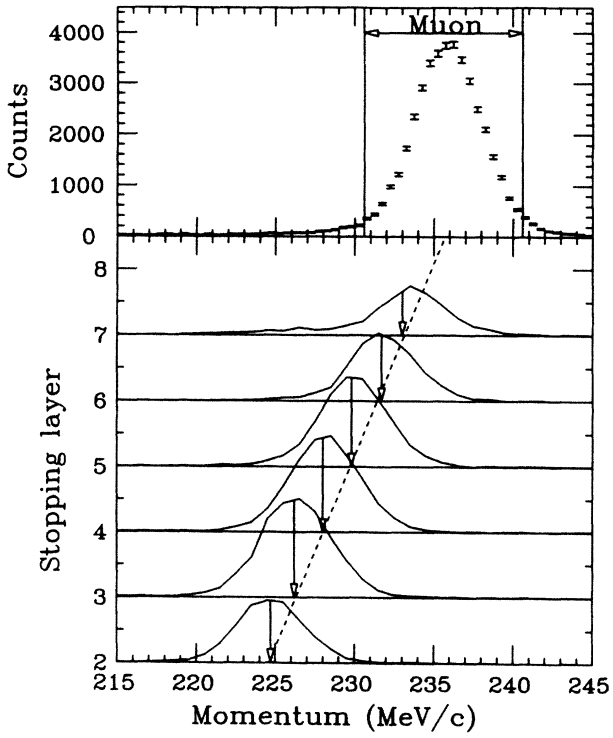

FIG. 10. The observed momentum of the muons is plotted for each kaon-stopping layer. The arrow indicates the averaged momentum of the muon. The dashed line shows the fitted momentum as a function of the kaon-stopping layer. The top of the figure shows the momentum distribution after the stopping layer correction. This was obtained by projecting the momentum to layer 8.5 (surface of the $T0$) along the dashed line.

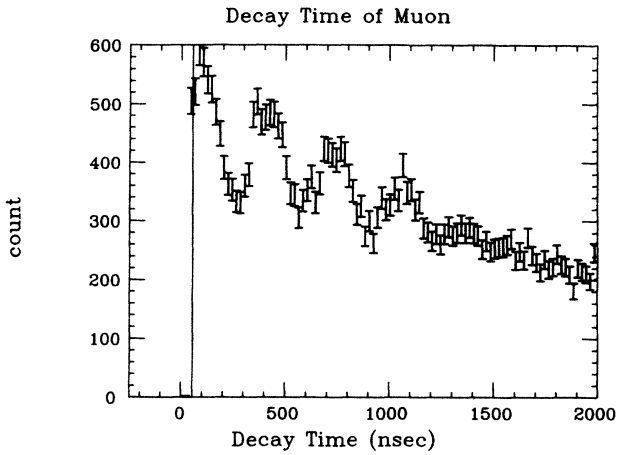

FIG. 11. The number of muon-decay positrons is shown as a function of decay time. The precession damps due to the inhomogeneity of the precession field.

V. ANALYSIS

After the data reduction, the polarization of the muon was obtained by the following three steps: (1) make a precession pattern with the raw data; (2) generate pure $V-A$ Monte Carlo events, and apply the same analysis to obtain the precession pattern; (3) fit the precession patterns with a cosine function and compare the amplitude to estimate the asymmetry.

A. Precession pattern of the experimental data

Figure 11 shows the number of observed positrons as a function of the decay time. This is roughly the same as (7), but we see a significant damping of the precession pattern caused by the inhomogeneity of the magnetic field over the Al target; as shown in Fig. 12, the magnetic field for the finally available events was distributed from 190 to 270 G.

In order to make the precession period independent of the magnetic field, a "precession angle" was introduced. This is the angle that the muon spin had rotated before the decay, which can be expressed as

$$\Theta = \omega(B)t - \phi , \tag{9}$$

where B is the magnetic field at the decay point and t is the decay time of the muon. For each event, the magnetic field was determined from the decay position and the field map.

The exponential decay term was removed to make the precession amplitude visible. If the magnetic field was uniform, then the exponential term would be

$$dD(\Theta) = n_0 \exp\left[-\frac{\Theta}{\omega\tau}\right] d\Theta . \tag{10}$$

In our case, the field was not uniform, and the *weight* of

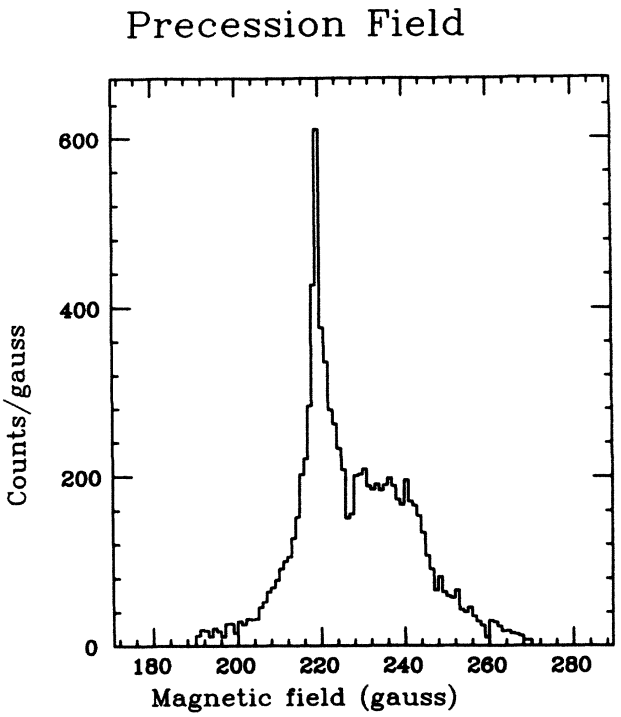

FIG. 12. Spin-precession magnetic-field distribution for the finally available events. The peak at 220 G is due to the events in which muons stopped in the central area of the target, where the field was uniform.

the field B had a distribution $n(B)$, so we have to take a convolution over B as

$$dD(\Theta)=d\Theta\int n(B)\exp\left[-\frac{\Theta}{\omega(B)\tau}\right]dB\ . \tag{11}$$

Then the precession term was obtained by

$$dA(\Theta)=dN(\Theta)/dD(\Theta)-1\ . \tag{12}$$

The data after this correction is shown in Fig. 13. As we see in the figure, the amplitude is less than the prediction of the pure $V-A$ hypothesis, $\frac{1}{3}$. This is because we are measuring the *projected* angle (muon-spin vector projected on the plane perpendicular to the spin-precession field) between muon spins and positrons.

B. Monte Carlo simulations

A Monte Carlo simulation was used to estimate the full precession amplitude of the pure $V-A$ events measured by this experimental setup. In generating the simulated events, the following points were taken into account.

(1) In order to reproduce the same distribution on the muon injection angle and the decay positron, those parameters were obtained from the real experimental data.

(2) The decay time of the muon was determined to follow the exponential distribution.

(3) The energy and the direction of the decay positron were determined to follow the pure $V-A$ theoretical distribution as given in (1).

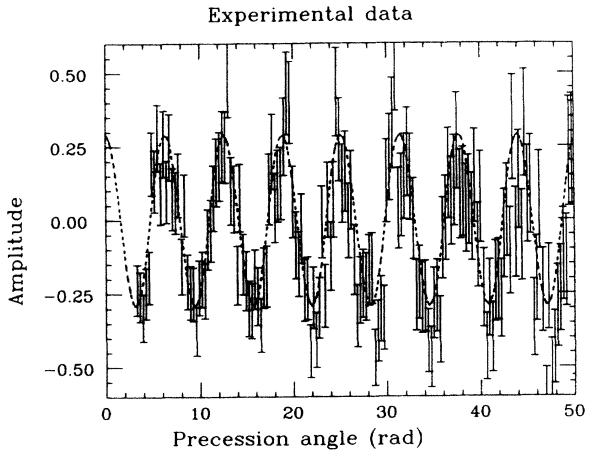

FIG. 13. The precession amplitude of the experimental data is shown as a function of the precession angle. The dotted line shows the best fit cosine function.

(4) The energy loss and the multiple scattering of the positron in the aluminum target were taken into account.

After the event generation, the events were selected and analyzed with the same parameters and procedures as the experimental data. The number of finally available events was 4×10^4. The simulated precession pattern is shown in Fig. 14.

C. Fitting the precession patterns

The muon polarization was calculated by comparing the precession amplitude of the experimental data and the Monte Carlo data. The amplitude α was obtained by fitting the precession patterns by a function

$$f(\Theta)=\alpha\cos(\beta\Theta+\gamma)\ . \tag{13}$$

Here, the β and γ are free parameters for fitting, which are expected to be 1.0 and 0.0, respectively. The patterns were fitted by minimizing the χ^2 value, where the error at each point was given by

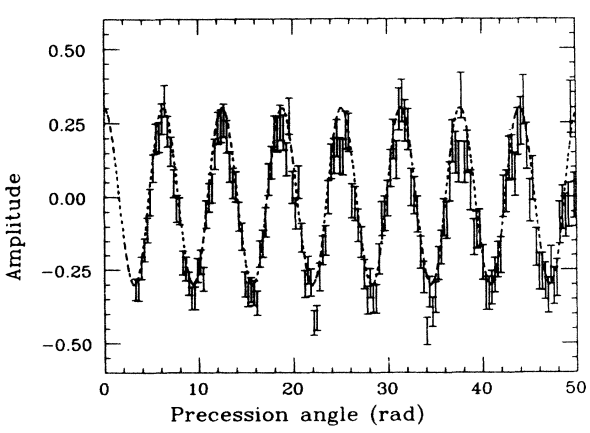

FIG. 14. Same as Fig. 13, except the plot is made for the Monte Carlo data.

$$\sigma(\Theta)=[dN(\Theta)]^{1/2}/dD(\Theta) . \quad (14)$$

The fitting was done in three regions: $\pi<\Theta<10\pi$, $\pi<\Theta<15\pi$, and $\pi<\Theta<20\pi$ with a binning width of 0.1π. Among these regions, the experimental data gave the minimum χ^2 value in the second region. The fitted curves are shown in Figs. 13 and 14 with dashed lines.

VI. RESULT

The fit within the range $\pi<\Theta<15\pi$ yielded $\alpha=0.292\pm0.013$ for the experimental data, while the Monte Carlo data predicted $\alpha_{MC}=0.304\pm0.006$ for 100% polarization. The normalized χ^2 were 1.23 and 1.18, respectively. The fit within a narrower range $\pi<\Theta<8\pi$ yielded the same result $\alpha=0.292\pm0.011$, indicating that there is no detectable polarization.

The following corrections were further applied to the Monte Carlo result α_{MC}, and we obtained $\alpha'_{MC}=0.301\pm0.006$.

(a) Depolarization of the 236-MeV/c μ^+ in the carbon degrader: 0.43%. As described in Appendix A, the spin of the relativistic muon is depolarized by the electric field of the carbon atoms.

(b) Multiple scattering of the muon in the kaon-stopping counters: 0.06%. If the muon suffered Coulomb scattering, then the muon direction was no longer parallel to the spin direction. It is impossible to know whether the muon was scattered in the stopping counters, i.e., before MWPC1.

(c) Background events which could not be rejected: 0.1%. In order to reject background particles which were not emitted from the muon-stopping target, the target area was surrounded by anticounters. Also a software cut was applied on the source point of the positrons. Even after those rejections, there was 0.1% of contamination of particles which came from behind the precession target. This was checked by taking data with the coincidence of the positron arm counters and the MWPC's.

(d) Radiative correction to the positron asymmetry in the muon decay: 0.3%.

As described in Appendix C, the energy spectrum of the muon is affected by the radiative correction of the muon decay. After integrating over the energy spectrum, this reduces the asymmetry at the level of 0.3%. This correction is needed because it was not included in the Monte Carlo simulation.

To the present level of precision, the muon decay parameter ξ can safely be set equal to 1.00 from the TRIUMF π-μ-e experiments.[9,10] Then, the muon polarization is obtained as

$$P_\mu \approx \xi P_\mu = -\alpha_{expt}/\alpha'_{MC} = -0.970\pm0.047 . \quad (15)$$

If we take the 90% confidence level, then the muon polarization is limited to be

$$|P_\mu| \approx \xi |P_\mu| > 0.902 . \quad (16)$$

VII. DISCUSSION AND CONCLUSION

Although the result was consistent with the $V-A$ hypothesis, we can set a new limit on the mass of the weak gauge boson and the Cabibbo angle in the right-handed sector. Here, we will assume that the mass of the right-handed neutrino to be less than 67 MeV/c^2, which corresponds to momentum cut at 230.5 MeV/c in the decay $K^+\to\mu^+\nu$. The mixing of *heavy* right-handed neutrino [$67<m(\nu_R)<300$ MeV/c^2] was excluded to an order of 10^{-4}–10^{-5} from our previous heavy-neutrino search experiment,[28] and recent heavy-neutrino decay experiments set stringent limits for heavier neutrinos.[29]

Generally, the overall coupling constant of the decay $K^+\to\mu^+\nu$ is proportional to $(g/m)^2\sin\theta$, where g is the weak coupling constant, m is the mass of the weak gauge boson, and θ is a quark-mixing (Cabibbo) angle. In the left-right-symmetric model, the left- and right-handed sectors may have their own m and θ parameters. The decay rate through the left- and right-handed currents can then be expressed as[30]

$$\Gamma_L \propto [(g/m_L)^2\sin\theta_L]^2 , \quad \Gamma_R \propto [(g/m_R)^2\sin\theta_R]^2 , \quad (17)$$

where the suffix L and R denote the left- and right-handed sectors, respectively. The polarization of the muon is thus

$$P_{K\mu} = -(\Gamma_L-\Gamma_R)/(\Gamma_L+\Gamma_R) \approx -1+2\Gamma_R/\Gamma_L = -1+2[(m_L/m_R)^2(\sin\theta_R/\sin\theta_L)]^2 . \quad (18)$$

The muon decay asymmetry ξ is expressed in the left-right-symmetric model as[31]

$$\xi = \frac{1-(m_L/m_R)^4}{1+(m_L/m_R)^4} \approx 1-2(m_L/m_R)^4 . \quad (19)$$

The product $\xi P_{K\mu}$ is thus

$$\xi P_{K\mu} \approx -1+2(m_L/m_R)^4[1+(\sin\theta_R/\sin\theta_L)^2] . \quad (20)$$

Since we obtained $\xi|P_{K\mu}|>0.902$, we conclude that the mass of the gauge boson and the Cabibbo angle in the right-handed sector is limited to

$$(m_L/m_R)^4[1+(\sin\theta_R/\sin\theta_L)^2]<0.049 \quad (21)$$

with a 90% confidence level.

Figure 15 shows the current 90% confidence limits on the ratios m_L/m_R and $\sin\theta_R/\sin\theta_L$. The vertical dashed line shows the limit on the Cabibbo-angle ratio obtained from the present θ_L value.[32] The upper dashed line is given from the pion decay experiment by Akhmanov *et al.*[11] The limit is calculated by the expression

$$\xi P_{\pi\mu} \approx -1+2(m_L/m_R)^4[1+(\cos\theta_R/\cos\theta_L)^2] . \quad (22)$$

Since $\cos\theta_L$ is nearly equal to 1 (0.97), pion decay is less sensitive to the right-handed Cabibbo angle. The bold solid curve is the upper limit given by our experiment. We see that our result has reduced the allowed regions

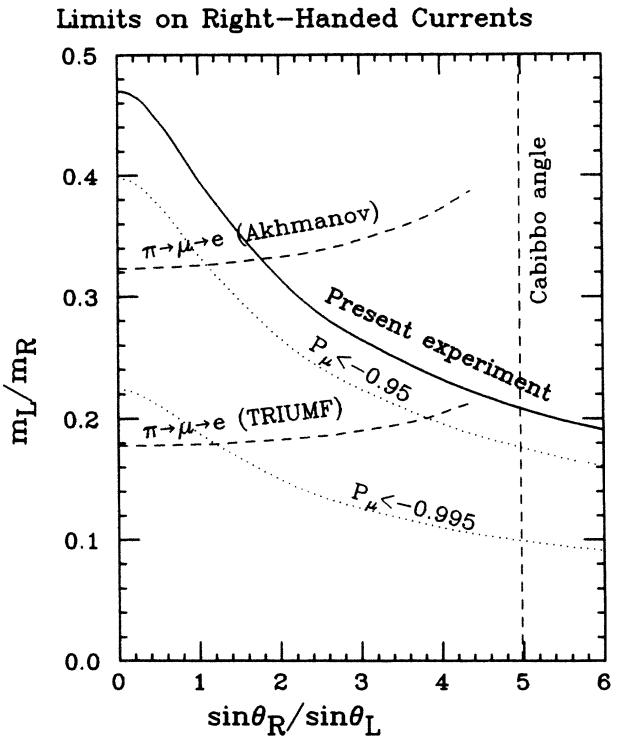

FIG. 15. Experimental 90% confidence limits on the m_L/m_R and $\sin\theta_R/\sin\theta_L$. The allowed regions are those which include the origin of the coordinate.

given by the above two limits. The lower dashed line represents the result of the recent muon-decay-asymmetry measurements at TRIUMF (Refs. 9 and 10). Their measurement $\xi |P_{\pi\mu}| \delta/\rho > 0.9966$ has set a limit $m_L/m_R < 0.20$ (lower dashed line), which is consistent with our result.

The present experiment has set a new limit on the mixture of right-handed currents as

$$(m_L/m_R)^4[1+(\sin\theta_R/\sin\theta_L)^2] < 0.049 \quad (90\%\ \text{C.L.}) .$$

It is of great interest to repeat this type of experiment with higher statistics and accuracy to check a discrepancy from the $V-A$ hypothesis, which will give direct information on the existence of $V+A$ currents, the right-handed gauge-boson mass, the right-handed Cabibbo angle, and the mass of neutrino.

It should be noted that most of the error in our experiment was caused by statistics, and the systematic error was less than 0.5%. Therefore, if we improve the acceptance of positron by a factor of 10, by covering the muon-stopping target with a cylindrical chamber, we can lower the limit to -0.95 (upper dotted curve in Fig. 15). If the primary kaon intensity and the acceptance of kaon decay can be increased by a factor 10^3–10^4 larger than in the present experiment, an upper limit will become -0.995 (lower dotted curve), and a deviation from the pure left handedness as small as 0.5% can be detected. Such a precision experiment may reveal the unknown world of the right-handed sector.

TABLE III. The magnitude of spin depolarization of the 236-MeV/c muons in the degrader.

Material	Z	$(-dE/dt)_{\min}$ (MeV)	η (%)	Range (cm)
C	6	75.8	0.43	37.4
Al	13	38.9	0.83	24.0
Fe	26	20.4	1.60	9.0
Cu	29	18.4	1.70	8.3
Pb	82	7.17	4.50	8.6

ACKNOWLEDGMENTS

We would like to thank Dr. T. Oka for his fruitful advice and suggestions on the theoretical aspects of this experiment. We are grateful to Professor T. Fujii and Professor T. Kamae of University of Tokyo, and Professor T. Nishikawa, Professor S. Ozaki, Professor A. Kusumegi, and Professor H. Sugawara of KEK, for their encouragement and support during the course of this experiment. Thanks are also due to the operating crew of the KEK proton synchrotron and its experimental facilities for their cooperation during the experiment.

APPENDIX A: DEPOLARIZATION OF MUON IN THE CARBON DEGRADER

At nonrelativistic velocities, the direction of muon spin is only affected by a magnetic field. Although a particle is deflected by the electric field of nuclei and electrons in a medium, the initial spin direction is still conserved. However, for a muon at relativistic speed, this electric field acts as a magnetic field perpendicular to the electric field and the particle direction. Therefore, the spin will rotate in the same plane as deflection, and thus will depolarize. The degree of depolarization, $\eta(\gamma_0)$, of a particle with an incident $\gamma=\gamma_0$ until it stops, was calculated theoretically[33] as

$$\eta(\gamma_0) < \frac{z^2M^2}{4m} \frac{1}{(-dE/dt)_{\min}} \frac{(\gamma_0-1)}{(\gamma_0+1)} , \tag{A1}$$

where $M=21$ MeV, m is the particle mass, and $(-dE/dt)_{\min}=L_r(-dE/dx)_{\min}$, which is the minimum energy loss per radiation length L_r. The $\eta(\gamma_0)$ of 235.5-MeV/c muon in lead is 4.4%, and for other media x this can be scaled by

$$\eta^x=\eta^{\text{Pb}}[(-dE/dt)^{\text{Pb}}_{\min}/(-dE/dt)^x_{\min}] . \tag{A2}$$

In Table III, η and the range of 235.5-MeV/c muon in some materials are given. Among them, carbon was the best choice for the degrader to minimize the depolarization effect.

APPENDIX B: DESIGN OF MWPC'S

In our experiment, six MWPC's (MWPC1–MWPC6) were used to reconstruct the particle trajectory. The anode and cathode wires were made of 20-μm-thick gold-plated tungsten wires and 100-μm-thick copper beryllium wires, respectively. The anode plane was placed between the two cathode planes. Two cathode planes had their wires perpendicular to each other. We read out induced

charges on both cathode planes, to obtain the hit position in both directions.

The output of each cathode strip of MWPC1 and MWPC2 was fed into an ADC through a preamplifier. For the rest of the chambers, the charge-division method was employed to reduce the number of ADC's. Cathode strips were connected to neighboring strips via registers, and readout channels were provided for every 11 strips.

APPENDIX C: RADIATIVE CORRECTION TO THE MUON DECAY

In evaluating the decay asymmetry of muons, we have to take into account two kinds of radiative corrections. One is caused by virtual photons, and the other is originated from real photon emission. The latter is called the radiative decay of the muon: $\mu \rightarrow e\nu\bar{\nu}\gamma$ with a branching ratio of 1.4% (Ref. 12). This decay should be included in the correction, since we could not distinguish it from the ordinal $\mu \rightarrow e\nu\bar{\nu}$ decay.

Although the radiative correction modifies the spectrum at the end-point energy,[34] the integrated asymmetry A_{int}^{r} does not differ as shown in Fig. 3. In our experiment, the energy threshold of the "decay e" logic was less than 1 MeV, which corresponds to $x < 0.02$. Therefore, the radiative correction reduced the asymmetry by 0.3%.

---

*Present address: Physics Department Fermi National Accelerator Laboratory, P.O. Box 500, Batavia, IL 60510.

†Present address: National Laboratory for High Energy Physics, Oho-machi, Tsukuba-gun, Ibaraki 305, Japan.

‡Present address: Science and Technology Agency, 2-2-1 Kasumigaseki, Chiyoda-ku, Tokyo 100, Japan.

§Present address: Rutgers University, New Brunswick, NJ 08903.

[1]S. L. Glashow, Nucl. Phys. **22**, 579 (1961).

[2]S. Weinberg, Phys. Rev. Lett. **19**, 1264 (1967).

[3]A. Salam, in *Elementary Particle Physics: Relativistic Groups and Analyticity,* edited by N. Svartholm (Almqvist and Wiksell, Stockholm, 1968), p. 367.

[4]M. Goldhaber, L. Grodzins, and A. W. Sunyar, Phys. Rev. **109**, 1015 (1958).

[5]G. Backenstoss *et al.*. Phys. Rev. Lett. **6**, 415 (1961).

[6]T. Yamazaki *et al.*, Phys. Rev. Lett. **39**, 1462 (1977).

[7]P. Truttmann *et al.*., Phys. Lett. **83B**, 48 (1979).

[8]J. C. Pati and A. Salam, Phys. Rev. Lett. **31**, 661 (1973); M. A. Bég, R. V. Budny, R. Mohapatra, and A. Sirlin, *ibid.* **38**, 1252 (1977).

[9]J. Carr *et al.*, Phys. Rev. Lett. **51**, 627 (1983).

[10]D. P. Stoker *et al.*, Phys. Rev. Lett. **54**, 1887 (1985).

[11]V. V. Akhmanov *et al.*, Yad. Fiz. **6**, 316 (1967) [Sov. J. Nucl. Phys. **6**, 230 (1968)].

[12]Particle Data Group, Rev. Mod. Phys. **56**, S1 (1984).

[13]C. A. Coombes *et al.*, Phys. Rev. **108**, 1348 (1957).

[14]D. Cutts, T. Elioff, and R. Stiening, Phys. Rev. **138**, B969 (1965).

[15]D. Cutts, R. Stiening, and C. Wiegand, Phys. Rev. **184**, 1380 (1969).

[16]R. S. Hayano *et al.* Phys. Rev. Lett. **52**, 329 (1984).

[17]R. H. Heffner *et al.*, Hyperfine Interact. **4**, 838 (1978).

[18]V. G. Grebinnik *et al.*, Pis'ma Zh. Eksp. Teor. Fiz. **27**, 33 (1978) [JETP Lett. **27**, 30 (1978)].

[19]O. Hartmann *et al.*, Phys. Rev. Lett. **44**, 337 (1980).

[20]T. O. Niinikoski *et al.*, Physica **108B**, 879 (1981).

[21]H. Schilling *et al.*, J. Phys. F **12**, 875 (1982).

[22]V. G. Grebinnik *et al.*, Zh. Eksp. Teor. Fiz. **75**, 1980 (1978) [Sov. Phys. JETP **48**, 1002 (1978)].

[23]M. Leon, *Exotic Atoms '79,* proceedings of the Second Course of the International School of Physics of Exotic Atoms, Erice, 1979, edited by K. Crowe, J. Duclos, G. Fiorentini, and G. Torelli (Plenum, New York, 1980), p. 327.

[24]H. K. Birnbaum *et al.*, Phys. Rev. B **17**, 4143 (1978).

[25]S. Kurokawa, H. Hirabayashi, and E. Kikutani, Nucl. Instrum. Methods **212**, 91 (1983).

[26]R. S. Hayano and J. Chiba, Report No. KEK Internal 82-3, 1982 (unpublished); Butsuri **37**, 936 (1982).

[27]J. Chiba *et al.*, Nucl. Instrum. Methods **206**, 451 (1983).

[28]R. S. Hayano *et al.*, Phys. Rev. Lett. **49**, 1305 (1982).

[29]A. M.Sarker-Cooper, *Proceedings of the XXII International Conference on High Energy Physics, Leipzig, 1984,* edited by A. Meyer and E. Wieczorek (Akademie der Wissenschaften der DDR, Zeuthen, DDR, 1984), p. 263.

[30]T. Oka, Phys. Rev. Lett. **50**, 1423 (1983).

[31]T. Oka (private communication).

[32]R. E. Shrock and L.-L. Wang, Phys. Rev. Lett. **41**, 1692 (1978).

[33]V. L. Lyuboshits, Yad. Fiz. **32**, 702 (1980) [Sov. J. Nucl. Phys. **32(3)**, 362 (1980)].

[34]W. E. Fischer and F. Scheck, Nucl. Phys. **B83**, 25 (1974).